

# S<sup>2</sup>MVTC: a Simple yet Efficient Scalable Multi-View Tensor Clustering

Zhen Long\*, Qiyuan Wang\*, Yazhou Ren, Yipeng Liu, Ce Zhu<sup>†</sup>

University of Electronic Science & Technology of China

eczhu@uestc.edu.cn

## Abstract

*Anchor-based large-scale multi-view clustering has attracted considerable attention for its effectiveness in handling massive datasets. However, current methods mainly seek the consensus embedding feature for clustering by exploring global correlations between anchor graphs or projection matrices. In this paper, we propose a simple yet efficient scalable multi-view tensor clustering (S<sup>2</sup>MVTC) approach, where our focus is on learning correlations of embedding features within and across views. Specifically, we first construct the embedding feature tensor by stacking the embedding features of different views into a tensor and rotating it. Additionally, we build a novel tensor low-frequency approximation (TLFA) operator, which incorporates graph similarity into embedding feature learning, efficiently achieving smooth representation of embedding features within different views. Furthermore, consensus constraints are applied to embedding features to ensure inter-view semantic consistency. Experimental results on six large-scale multi-view datasets demonstrate that S<sup>2</sup>MVTC significantly outperforms state-of-the-art algorithms in terms of clustering performance and CPU execution time, especially when handling massive data. The code of S<sup>2</sup>MVTC is publicly available at <https://github.com/longzhen520/S2MVTC>.*

## 1. Introduction

The progress in information collection technology now permits us to gather multi-view data from the same object, presenting observations with depth and comprehensiveness. For instance, brain activity can be measured using functional Magnetic Resonance Imaging (fMRI) and Electroencephalography (EEG) [11, 26]. Benefiting from the consensual and complementary information, multi-view data have attracted a series of multi-view learning tasks [1, 32]. Among them, multi-view clustering, which groups data

into several clusters by integrating information from different views, has been extensively applied in fields including image processing, computer vision, and neuroscience [3, 29, 36, 43].

Current multi-view clustering (MVC) methods, mainly based on self-representation learning or graph learning, aim to find the consensus embedding feature and have attained considerable advancements [4, 22, 24, 31]. However, for  $V$  views and  $N$  samples, these methods require updating  $V$  membership graphs ( $N \times N$ ) to construct the affinity matrix, which will be then fed into spectral clustering algorithm [34]. Both storage and computational demands for these methods scale at a complexity of  $O(VN^3)$ , where  $V$  and  $N$  represent the numbers of views and samples, respectively. These methods could be infeasible for large-scale datasets, particularly when  $N$  is massive, and such scalability is important in real-world applications.

To address it, many anchor-based scalable MVC methods have been proposed for large-scale data [20, 30, 37, 42], where  $V$  anchor graphs of size  $M \times N$  are constructed from  $M$  anchors and  $N$  samples ( $M \ll N$ ) to approximately represent  $V$  memberships between multi-view data. According to the differences in inter-view processing levels, these methods can be further subdivided into two categories. The first one relies on anchor learning, emphasizing the exploration of anchor graph consistency across views, as shown in Fig. 1 (a). Subsequently, the fused anchor graph is employed to construct the embedding feature, which will be fed into a  $k$ -means algorithm for clustering [12, 24, 39, 42]. The second one relies on provided anchor graphs and learns the embedding feature using the projection matrices, as shown in Fig. 1 (b). It explores the consistency among projection matrices to acquire the compact embedding feature, which is then utilized for learning clustering structures [35, 44, 45].

The above-mentioned anchor-based methods either explore the global correlations between anchor graphs or projection matrices. However, their ultimate goal is to learn the consensus embedding feature, which directly impacts the clustering performance. Therefore, two questions naturally arise: Why not directly explore the correlations be-

\*Equal contribution.

<sup>†</sup>Corresponding author. This work is supported by the National Natural Science Foundation of China (NSFC) under Grant 62020106011.

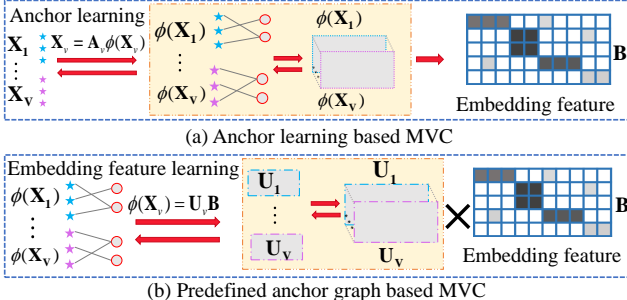


Figure 1. Comparison frameworks of current methods.

tween embedding features from different views? Would this approach be more effective?

In this paper, we try to answer these questions and focus on learning inter-and intra-view consistency among embedding features. We propose a simple yet efficient scalable multi-view tensor clustering (S<sup>2</sup>MVTC) approach tailored for large-scale data. As depicted in Fig. 2, we initially map the anchor graph  $\phi(\mathbf{X}_v) \in \mathbb{R}^{M \times N}$  onto the projection matrix  $\mathbf{U}_v$  to obtain the embedding feature  $\mathbf{B}_v \in \mathbb{R}^{K \times N}$  for each view. To ensure the consensus among intra-view embedding features effectively, we introduce a novel approach by employing a tensor low-frequency approximation (TLFA) on the embedding feature tensor, denoted as  $\mathcal{B} \in \mathbb{R}^{K \times V \times N}$ , where the tensor is formed by concatenating the embedding features from each view and subsequently rotating it. Benefiting from the fast Fourier transform (FFT) in the third mode of tensor singular value decomposition (t-SVD) [15], the newly defined TLFA can achieve the smooth representation of samples within different views [8].

Furthermore, to ensure inter-view semantic consistency, a consensus constraint is imposed on the embedding features. By incorporating these two parts into a unified framework, S<sup>2</sup>MVTC can efficiently leverage inter/intra-view information for large-scale MVC tasks. Ultimately, the clustering structure learning is applied to the well-learned embedding consensus feature  $\tilde{\mathbf{B}}$  to obtain the clustering results. The main contributions are summarized as:

- Different from existing anchor-based methods that explore global correlations between anchor graphs or projection matrices, S<sup>2</sup>MVTC directly learns both inter and intra-view embedding feature correlations.
- Benefiting from the newly defined TLFA operator, S<sup>2</sup>MVTC achieves the smooth representation within different views.
- Experimental results on six large multi-view datasets demonstrate that S<sup>2</sup>MVTC significantly improves the clustering performance compared to state-of-the-art algorithms, especially as the data size increases, making the advantages of S<sup>2</sup>MVTC more evident.

## 2. Notations and Problem Formulation

### 2.1. Notations

For clarity, we present notations frequently used in Tab. 1.

Table 1. Summary of notations in this paper.

Symbol	Definition
$x, \mathbf{x}, \mathbf{X}$ , and $\mathcal{X}$	A scalar, a vector, a matrix, and a tensor
$v = 1, \dots, V$	Indices range from 1 to their capital version
$\mathbb{R}, \mathbb{C}$	Fields of real numbers and complex numbers
$\text{conj}(\mathcal{X})$	the complex conjugate of $\mathcal{X}$
$[x]$	the one greater than or equal to $x$
$\mathcal{X} \in \mathbb{R}^{I_1 \times I_2 \times I_3}$	A 3-rd order tensor
$\mathcal{X}(:, :, i_3)$	the $i_3$ -th frontal slice of $\mathcal{X}$
$N, V, C, M$	Number of samples, views, clusters, anchors
$\phi(\mathbf{X}_v) \in \mathbb{R}^{M \times N}$	Anchor graph in the $v$ -th view
$\mathbf{U}_v \in \mathbb{R}^{M \times K}$	Projection matrix in the $v$ -th view
$\mathbf{B}_v \in \mathbb{R}^{K \times N}$	embedding feature in the $v$ -th view
$\mathcal{B} \in \mathbb{R}^{K \times V \times N}$	The rotated embedding feature tensor

### 2.2. Preliminaries on t-SVD

**Definition 1 (T-product [27])** The T-product of two third-order tensors  $\mathcal{X} \in \mathbb{R}^{I_1 \times I_2 \times I_3}$  and  $\mathcal{Y} \in \mathbb{R}^{I_2 \times J \times I_3}$  is defined as

$$\mathcal{Z} = \mathcal{X} * \mathcal{Y} \in \mathbb{R}^{I_1 \times J \times I_3}, \quad (1)$$

which can be computed by multiple matrix multiplication operations in the Fourier transform domain.

**Definition 2 (Tensor transpose [15])** Under the Fourier transform, the conjugate transpose of a tensor  $\mathcal{X} \in \mathbb{C}^{I_1 \times I_2 \times I_3}$  is denoted as  $\mathcal{X}^T \in \mathbb{C}^{I_2 \times I_1 \times I_3}$ . It satisfies

$$\mathcal{X}^T(:, :, 1) = (\mathcal{X}(:, :, 1))^T, \quad (2)$$

and

$$\mathcal{X}^T(:, :, i_3) = (\mathcal{X}(:, :, I_3 + 2 - i_3))^T, i_3 = 2, \dots, I_3, \quad (3)$$

where  $\mathcal{X}^T(:, :, i_3)$  is the  $i_3$ -th frontal slice of  $\mathcal{X}^T$ .

**Definition 3 (Orthogonal tensor) [15]** A tensor  $\mathcal{X}$  is called orthogonal when it satisfies

$$\mathcal{X} * \mathcal{X}^T = \mathcal{X}^T * \mathcal{X} = \mathcal{I}, \quad (4)$$

where  $\mathcal{I}$  is the identity tensor.

**Definition 4 (f-diagonal tensor) [16]** A tensor  $\mathcal{X} \in \mathbb{R}^{I_1 \times I_2 \times I_3}$  is called f-diagonal when each frontal slice  $\mathcal{X}^{(i_3)}$ ,  $i_3 = 1, \dots, I_3$  is a diagonal matrix.

**Definition 5 (tensor Singular Value Decomposition(t-SVD) [2, 15, 25])** For a tensor  $\mathcal{X} \in \mathbb{R}^{I_1 \times I_2 \times I_3}$ , its t-SVD is represented as:

$$\mathcal{X} = \mathcal{U} * \mathcal{S} * \mathcal{V}^T, \quad (5)$$

where  $\mathcal{U} \in \mathbb{R}^{I_1 \times I_2 \times I_3}$  and  $\mathcal{V} \in \mathbb{R}^{I_2 \times I_3}$  are orthogonal tensors, and  $\mathcal{S} \in \mathbb{R}^{I_1 \times I_2 \times I_3}$  is an f-diagonal tensor.

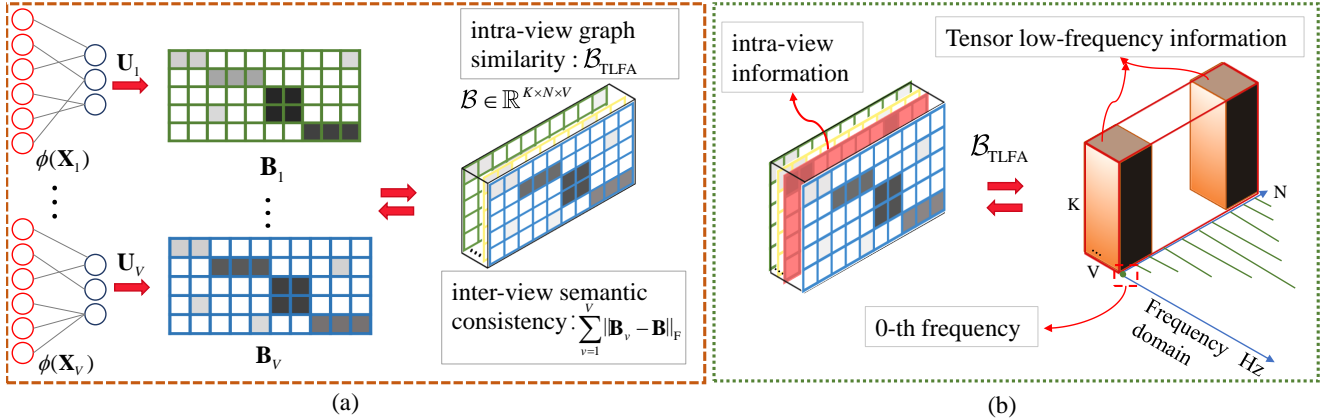


Figure 2. The framework of  $S^2$ MVTC. (a) The process involves mapping each pre-given anchor graph  $\phi(\mathbf{X}_v)$  using  $\mathbf{U}_v$  to obtain the corresponding embedding feature  $\mathbf{B}_v$ . These embedding features,  $\mathbf{B}_v$ , are then formed into a tensor  $\mathcal{B}$ . This tensor, along with the newly defined  $\mathcal{B}_{\text{TLFA}}$  and  $\sum_{v=1}^V \|\mathbf{B}_v - \tilde{\mathbf{B}}\|_F$ , are utilized to explore intra-view correlations and semantic consistency, respectively, where  $\tilde{\mathbf{B}} = \sum_{v=1}^V \frac{1}{V} \mathbf{B}_v$ . (b) The tensor low-frequency approximation  $\mathcal{B}_{\text{TLFA}}$ .

---

**Algorithm 1** t-SVD

---

**Input:**  $\mathcal{X} \in \mathbb{R}^{I_1 \times I_2 \times I_3}$ .  
**Output:**  $\mathcal{U} \in \mathbb{R}^{I_1 \times I_1 \times I_3}$ ,  $\mathcal{S} \in \mathbb{R}^{I_1 \times I_2 \times I_3}$ ,  $\mathcal{V} \in \mathbb{R}^{I_2 \times I_2 \times I_3}$ ;  
 $\hat{\mathcal{X}} \leftarrow \text{fft}(\mathcal{X}, [], 3)$ ;  
 $[\mathbf{U}, \mathbf{S}, \mathbf{V}] = \text{svd}(\hat{\mathcal{X}}(:, :, 1))$ .  
**for**  $i_3 = 1$  to  $I_3$  **do**  
     $[\mathbf{U}, \mathbf{S}, \mathbf{V}] = \text{svd}(\hat{\mathcal{X}}(:, :, i_3))$ ;  
     $\hat{\mathcal{U}}(:, :, i_3) = \mathbf{U}; \hat{\mathcal{S}}(:, :, i_3) = \mathbf{S}; \hat{\mathcal{V}}(:, :, i_3) = \mathbf{V}$ .  
**end for**  
 $\mathcal{U} = \text{ifft}(\hat{\mathcal{U}}, [], 3); \mathcal{S} = \text{ifft}(\hat{\mathcal{S}}, [], 3); \mathcal{V} = \text{ifft}(\hat{\mathcal{V}}, [], 3)$ .

---

According to the T-product operation in Definition 1, this decomposition can be obtained by Algorithm 1, where fft and ifft are the fast Fourier transform (FFT) operator and the inverse FFT, respectively.

## 2.3. Related works

### 2.3.1 Anchor learning for large-scale MVC

The general framework of an anchor-learning-based large-scale MVC is constructed as follows:

$$\begin{aligned} & \min_{\{\mathbf{Z}_v\}_{v=1}^V} \sum_{v=1}^V \|\mathbf{X}_v - \mathbf{A}_v \mathbf{Z}_v\|_F^2 + \lambda \Psi(\mathbf{Z}_v) \\ & \text{s. t. } \mathbf{Z}_v^T \mathbf{1} = 1, \mathbf{Z}_v \geq 0, v = 1, \dots, V, \end{aligned} \quad (6)$$

where  $\mathbf{A}_v \in \mathbb{R}^{D_v \times M}$  is the learned anchor matrix in the  $v$ -th view and  $M$  is the number of anchors.  $\mathbf{Z}_v \in \mathbb{R}^{M \times N}$  is the anchor graph, which is used to describe the relationship among samples. In addition,  $\Psi(\mathbf{Z}_v)$  represents the regularization terms. Kang *et al.* [14] consider Frobenius norm

on  $\mathbf{Z}_v$  to find a stable solution for large-scale MVC. However, the anchor graph in each view is learned separately, failing to explore the complementary information. To solve this, many fusion strategies are considered to find the consensus representation among views. For example, Liu *et al.* [39] considered the respective projection matrix to find the consistent graph. Li *et al.* [21] considered the joint graph across multiple views via a self-supervised weighting manner. Chen *et al.* [5] introduced the Fast Self-guided Multi-view Subspace Clustering algorithm, which effectively combines view-shared anchor learning and global-guided-local self-guidance learning into a comprehensive model. Huang *et al.* [9] considered three levels of diversity: features, anchors, and neighbors. By leveraging these levels of diversity, view-sharing bipartite graphs are constructed, enhancing the effectiveness of the clustering process. In addition, some methods based on tensor anchor graphs have been proposed [12, 24, 42]. These methods stack each anchor graph into a tensor and use low-rank tensor approximation to integrate the consistency information among anchor graphs across views, achieving good performance on large-scale data.

### 2.3.2 Embedding feature learning for large-scale MVC

Unlike large-scale MVC methods based on anchor learning, another approach focuses on learning embedding features through the pre-defined anchor graphs in the pre-processing step. Typically, these anchor graphs are constructed using kernel mapping, for instance, through nonlinear Radial Basis Function (RBF) mapping, as follows:

$$\phi(\mathbf{x}_v^n) = [\exp(-\frac{\|\mathbf{x}_v^n - \mathbf{z}_v^1\|^2}{\sigma}), \dots, \exp(-\frac{\|\mathbf{x}_v^n - \mathbf{z}_v^M\|^2}{\sigma})]^T, \quad (7)$$

where  $\sigma$  is the kernel width,  $\mathbf{z}_v^m \in \mathbb{R}^{D_v}$ ,  $m = 1, \dots, M$  are anchors, which randomly chooses from the column of  $v$ -th view  $\mathbf{X}_v \in \mathbb{R}^{D_v \times N}$ .  $\phi(\mathbf{x}_v^n) \in \mathbb{R}^M$  represents the non-linear relationship between  $M$  anchors and the  $n$ -th samples. In this way, Zhang *et al.* [45] projected non-linear anchor graphs from different views to a common Hamming feature space. This shared feature space is then fed into binary clustering structure learning to derive the final clustering results. However, this method solely explores pairwise correlations between views. To uncover global correlations among views, Zhang *et al.* [44] considered consistent projections, obtained by low-rank tensor approximation, to find a better binary feature representation for large-scale MVC tasks. Additionally, Wang *et al.* [35] considered autoencoder learning techniques to find consistent projections for generating binary features used in clustering.

### 3. Methods

As mentioned above, anchor-based methods mostly focus on learning high-order information between anchor graphs or projection matrices. However, their ultimate goal is to obtain shared embedding features across views.

#### 3.1. Model development

In this section, we will focus on how to quickly learn the consistency among embedding features well, which involves the exploration of intra-view graph similarity (IGS) and ensuring inter-view semantic consistency (ISC). With anchor graphs  $\phi(\mathbf{X}_v) \in \mathbb{R}^{M \times N}$ ,  $v = 1, \dots, V$  obtained in advance, we can first learn  $V$  embedding features by projection matrices  $\mathbf{U}_v$ ,  $v = 1, \dots, V$ , as follows:

$$\min_{\{\mathbf{U}_v, \mathbf{B}_v\}_{v=1}^V} \sum_{v=1}^V \frac{\lambda}{2} \|\mathbf{U}_v\|_F^2 + \frac{1}{2} \|\mathbf{B}_v - \mathbf{U}_v \phi(\mathbf{X}_v)\|_F^2 \quad (8)$$

$$\text{s. t. } \mathbf{B}_v(:, n) \in \mathbb{S}, n = 1, \dots, N, v = 1, \dots, V,$$

where  $\lambda$  serves as a weight aiming to attain a stable solution for the mapping matrix  $\mathbf{U}_v$ .  $\mathbf{B}_v(:, n) \in \mathbb{S}$  represents the  $z$ -score normalization constraint, ensuring that each feature from different views has a mean of 0 and a standard deviation of 1. Here  $\mathbf{b}_v^n = \mathbf{B}_v(:, n)$ , and  $\mathbb{S} = \{\mathbf{b}_v^n : \sum_{k=1}^K \mathbf{b}_v^n(k) = 0, \frac{\sum_{k=1}^K (\mathbf{b}_v^n(k))^2}{K-1} = 1, n = 1, \dots, N\}$ .

To efficiently explore the intra-view information of embedding features, we initially stack the embedding features from each view into a tensor. Subsequently, we introduce a newly tensor low-frequency approximation  $\|\mathcal{B}\|_{\text{TLFA}}$ , applied to its rotated form  $\mathcal{B} \in \mathbb{R}^{K \times V \times N}$ , aiming to capture the IGS.

**Definition 6 (Tensor low-frequency approximation (TLFA))** According to the  $t$ -SVD computation outlined in Algorithm 1, the TLFA of a tensor  $\mathcal{B} \in \mathbb{R}^{K \times V \times N}$  is

defined as the frontal slices in the low-frequency domain. Mathematically, it is expressed as:

$$\min_{\mathcal{Y}} \frac{1}{2} \|\mathcal{B} - \mathcal{Y}\|_F^2, \text{ s. t. } \mathcal{Y} = \text{ifft}(\widehat{\mathcal{Y}}, [], 3),$$

where  $\widehat{\mathcal{Y}} = \widehat{\mathcal{B}}(:, :, 1) + \sum_{n=2}^L (\widehat{\mathcal{B}}(:, :, n) + \widehat{\mathcal{B}}(:, :, N+2-n))$ .  $\widehat{\mathcal{B}} = \text{fft}(\mathcal{B}, [], 3)$ , means applying the fast Fourier transform along the sample (3-rd) dimension for the embedding features from different views. The obtained low-frequency components incorporate graph similarity into embedding feature learning, resulting in a smooth representation.

Besides, the term  $\sum_{v=1}^V \|\tilde{\mathbf{B}} - \mathbf{B}_v\|_F^2$  is included to ensure ISC [40], where  $\tilde{\mathbf{B}}$  is the average embedding feature.

Overall, the framework of S<sup>2</sup>MVTC is formulated as:

$$\begin{aligned} \min_{\{\mathbf{B}_v, \mathbf{U}_v\}_{v=1}^V, \tilde{\mathbf{B}}} & \sum_{v=1}^V \left( \frac{\lambda}{2} \|\mathbf{U}_v\|_F^2 + \frac{1}{2} \|\mathbf{B}_v - \mathbf{U}_v \phi(\mathbf{X}_v)\|_F^2 \right. \\ & \left. + \frac{\beta}{2} \|\tilde{\mathbf{B}} - \mathbf{B}_v\|_F^2 \right) + \tau \|\mathcal{B}\|_{\text{TLFA}} \\ \text{s. t. } & \tilde{\mathbf{B}}(:, n), \mathbf{B}_v(:, n) \in \mathbb{S}, n = 1, \dots, N, v = 1, \dots, V. \end{aligned} \quad (9)$$

Here  $\mathcal{B} = \Omega(\mathbf{B}_1, \dots, \mathbf{B}_V)$ , where  $\Omega$  represents the operation of stacking each feature and rotating and the inverse operator  $\mathbf{B}_v = \Omega_v^{-1}(\mathcal{B})$ .

To make the above optimization problem separable, we introduce an auxiliary variable  $\mathcal{Y}$ , leading to the reformulation as follows:

$$\begin{aligned} \min_{\{\mathbf{B}_v, \mathbf{U}_v\}_{v=1}^V, \tilde{\mathbf{B}}} & \sum_{v=1}^V \left( \frac{\lambda}{2} \|\mathbf{U}_v\|_F^2 + \frac{1}{2} \|\mathbf{B}_v - \mathbf{U}_v \phi(\mathbf{X}_v)\|_F^2 \right. \\ & \left. + \frac{\beta}{2} \|\tilde{\mathbf{B}} - \mathbf{B}_v\|_F^2 + \frac{1}{2} \|\mathcal{B} - \mathcal{Y}\|_F^2 + \tau \|\mathcal{Y}\|_{\text{TLFA}} \right) \\ \text{s. t. } & \tilde{\mathbf{B}}(:, n), \mathbf{B}_v(:, n) \in \mathbb{S}, n = 1, \dots, N, v = 1, \dots, V. \end{aligned} \quad (10)$$

#### 3.2. Solutions

This optimal problem in Eq. (10) can be solved through an alternating optimization approach, where each parameter is updated individually while keeping the others fixed.

**Update  $\mathbf{U}_v$ .** Fixing other variables, the subproblem of  $\mathbf{U}_v$  can be rewritten as:

$$\min_{\mathbf{U}_v} \frac{1}{2} \|\mathbf{B}_v - \mathbf{U}_v \phi(\mathbf{X}_v)\|_F^2 + \frac{\lambda}{2} \|\mathbf{U}_v\|_F^2. \quad (11)$$

By taking the derivative of the equation and setting it equal to zero, we can obtain:

$$\mathbf{U}_v = (\mathbf{B}_v \phi^T(\mathbf{X}_v))(\phi(\mathbf{X}_v) \phi^T(\mathbf{X}_v) + \lambda \mathbf{I})^\dagger, \quad (12)$$

where  $\phi(\mathbf{X}_v) \phi^T(\mathbf{X}_v)$  can be pre-calculated outside the main loop to decrease the computational cost. Therefore, the storage and computational complexity are  $O(MN)$  and

$O(\max(KMN, M^3))$ , respectively.

**Update  $\mathbf{B}_v$ .** The subproblem of  $\mathbf{B}_v$  can be rephrased as:

$$\begin{aligned} \min_{\mathbf{B}_v} \frac{1}{2} \|\mathbf{B}_v - \mathbf{U}_v \phi(x_v)\|_F^2 + \frac{\beta}{2} \|\tilde{\mathbf{B}} - \mathbf{B}_v\|_F^2 + \frac{1}{2} \|\mathcal{B} - \mathcal{Y}\|_F^2, \\ \text{s.t. } \mathbf{B}_v(:, n) \in \mathbb{S}, n = 1, \dots, N. \end{aligned} \quad (13)$$

Similarly, by taking the derivative of the equation and setting it equal to zero, we can obtain

$$\mathbf{B}_v = \text{normalize}(\beta \tilde{\mathbf{B}} + \Omega_v^{-1}(\mathcal{Y}) + \mathbf{U}_v \phi(\mathbf{x}_v)) / (\beta + 2), \quad (14)$$

where  $\Omega_v^{-1}(\mathcal{Y}) = \mathbf{Y}_v \in \mathbb{R}^{K \times N}$ . `normalize` is the  $z$ -score normalization function, which can be achieved by the Matlab command “`normalize`”. In this case, both the storage and computational complexity of updating  $\mathbf{B}_v$  are  $O(KN)$ .

**Update  $\mathcal{Y}$ .** The subproblem of  $\mathcal{Y}$  is rewritten as:

$$\min_{\mathcal{Y}} \tau \|\mathcal{Y}\|_{\text{TLFA}} + \frac{1}{2} \|\mathcal{B} - \mathcal{Y}\|_F^2. \quad (15)$$

According to the definition of  $\|\mathcal{Y}\|_{\text{TLFA}}$ , a closed-form solution for  $\mathcal{Y}$  can be obtained by choosing the low-frequency component in the Fourier domain. The details are outlined in Algorithm 2. The computational and storage complexity are  $O(KVN \log(N))$  and  $O(KNV)$ , respectively.

**Update  $\tilde{\mathbf{B}}$ .** The subproblem of updating  $\tilde{\mathbf{B}}$  is:

$$\min_{\tilde{\mathbf{B}}} \sum_{v=1}^V \frac{\beta}{2} \|\tilde{\mathbf{B}} - \mathbf{B}_v\|_F^2 \text{ s.t. } \tilde{\mathbf{B}}(:, n) \in \mathbb{S}, n = 1, \dots, N. \quad (16)$$

The solution of  $\tilde{\mathbf{B}}$  is:

$$\tilde{\mathbf{B}} = \text{normalize}\left(\frac{1}{V} \sum_{v=1}^V \mathbf{B}_v\right), \quad (17)$$

which needs computational and storage complexity of  $O(KN)$  and  $O(KNV)$ , respectively.

After obtaining the consistent fused embedding feature  $\tilde{\mathbf{B}}$ . The final clustering results can be obtained by the following clustering structure learning framework:

$$\min_{\mathbf{D}, \mathbf{G}} \|\tilde{\mathbf{B}} - \mathbf{D}\mathbf{G}\|_F^2 \text{ s.t. } \sum_{c=1}^C \mathbf{G}(c, :) = \mathbf{1}, \mathbf{G} \in \{0, 1\}, \quad (18)$$

where  $\mathbf{D}$  is the clustering center and  $\mathbf{G}$  is the clustering indicator matrix.

Overall, the method S<sup>2</sup>MVTC is summarized in Algorithm 3. According to the parameters analysis in the algorithm, the main storage and computational complexities of S<sup>2</sup>MVTC are  $O(\max(KVN, MN))$  and  $O(\max(KMNT, M^3T))$ , respectively, where  $T$  represents the total number of iterations in the S<sup>2</sup>MVTC.

In addition, the theoretical convergence can be well guaranteed. Our problem is bounded due to the summation of

---

### Algorithm 2 Updating $\mathcal{Y}$

---

**Input:**  $\mathbf{B}$ , low frequency parameter  $L$ .  
**Output:**  $\mathcal{Y}$ ;  
 $\tilde{\mathcal{B}} \leftarrow \text{fft}(\mathcal{B}, [], 3)$ ;  
 $\hat{\mathcal{Y}}(:, :, 1)) = \hat{\mathcal{B}}(:, :, 1))$ ;  
**for**  $n = 2$  to  $L$  **do**  
     $\hat{\mathcal{Y}}(:, :, n) = \hat{\mathcal{B}}(:, :, n)$ ;  
     $\hat{\mathcal{Y}}(:, :, N + 2 - n) = \text{conj}(\hat{\mathcal{Y}}(:, :, n))$ .  
**end for**  
 $\mathcal{Y} = \text{ifft}(\hat{\mathcal{Y}}, [], 3)$ .

---



---

### Algorithm 3 S<sup>2</sup>MVTC

---

**Input:** Anchor graphs  $\phi(\mathbf{X}_v), v = 1, \dots, V$ , low frequency parameter  $L$ , regularization parameters  $\beta, \lambda$ .  
**Initialize:**  $\tau = 1$ , Maximum iterations  $T = 7$ .  
**for**  $t = 1$  to  $T$  **do**  
    **for**  $v = 1$  to  $V$  **do**  
        Update  $\mathbf{U}_v$  via Eq. (12);  
        Update  $\mathbf{B}_v$  via Eq. (14);  
    **end for**  
        Update  $\mathcal{Y}$  via Eq. (15);  
        Update  $\tilde{\mathbf{B}}$  via Eq. (17);  
         $\tau = \tau * 1.1$ .  
**end for**  
    Apply Eq. (18) to find the clustering indicator matrix  $\mathbf{G}$ .  
**Output:** Clustering result.

---

norms with positive penalty parameters. Furthermore, the exact minimum points of each subproblem can be achieved, implying that each subproblem exhibits a monotone decrease. The proposed algorithm converges according to the convergence theorem in [28] (theorem 7.29).

## 4. Experiments

### 4.1. Experimental settings

**Multi-view Datasets:** Six well-known large-scale multi-view datasets, including **CCV** [13], **NUS-WIDE-OBJ** [7], **Caltech102** [19], **AwA** [18], **Cifar-10** [17], **Youtube-Face\_sel** [41] evaluate the effectiveness of S<sup>2</sup>MVTC, where the statistical information is presented in Tab. 2.

**Compared Clustering Algorithms.** To compare clustering performance, we select  $k$ -means and seven state-of-the-art methods: binary multi-view clustering (BMVC) [2018, TPMAI] [45], fast multi-View anchor-correspondence clustering (FMVACC) [2022, NeurIPS] [38], one-pass multi-view clustering (OPMC) [2021, ICCV] [23], fast multi-view clustering via ensembles (FastMICE) [2023, TKDE] [10], scalable and parameter-free multiview graph clustering (SFMC) [2020, TPMAI] [20], fast self-guided multi-

Datasets	#Sample	#Cluster	#View	# Feature
CCV	6773	20	3	20,20,20
Caltech102	9144	102	6	48,40,254,1984,512,928
NUS-WIDE-OBJ	30000	31	5	65,226,145,74,129
AwA	30475	50	6	2688,2000,252,2000,2000,2000
Cifar-10	50000	10	3	512,2048,1024
YoutubeFace_sel	101499	31	5	64,512,64,647,838

Table 2. Multi-view datasets used in our experiments.

view subspace clustering (FSMSC) [2023, TIP] [6], fast parameter-free multi-view subspace clustering with consensus anchor guidance (FPMVS-CAG) [2021, TIP] [37]. One low-rank tensor-based multi-view method: scalable low-rank MERA based multi-view clustering (sMERA-MVC) [2023, TMM] [24]. All tests were conducted on a desktop computer equipped with a 3.79GHz AMD Ryzen 9 3900X CPU and 64GB RAM, using MatLab 2021b.

**Evaluation Metrics.** To assess the performance in our experiments, eight standard evaluation metrics are utilized, including Accuracy (ACC), Normalized Mutual Information (NMI), Purity, F-score, Precision (PRE), Recall (REC), Adjusted Rand Index (ARI), and CPU Time. These metrics, except for CPU Time, are designed such that higher values signify superior clustering performance.

**Parameter Sensitivity Analysis.** In our experiment, we employed a grid search strategy to determine the optimal choices for all parameters. S<sup>2</sup>MVTC has a fixed parameter  $M$ , which is the size of the anchor, and three free parameters: low frequency parameter, denoted as  $L$ , and two balance parameters,  $\lambda$  and  $\beta$ . We fixed two of these parameters and adjusted the third through an exhaustive search. For instance in dataset Caltech102, we initially fixed  $L = 16$  and  $M = 1000$ , and adjusted parameters  $\beta$  and  $\lambda$ , where  $\beta$  and  $\lambda$  took values in  $\{10^{-4}, 10^{-3}, \dots, 10^2\}$ . The clustering results are shown in Fig. 3(a), where the performance remains stable with  $\beta$  in the range of  $[10^{-4}, 1]$ , with ACC close to 55.47%. We observed that the best clustering performance can be achieved within a wide range of  $\lambda$ , specifically  $\lambda \in [10^{-1}, 10^1]$ . Additionally, we fixed  $\beta = 1$  and  $\lambda = 10$ , and selected parameter  $M$  from  $\{500, 1000, \dots, 3000\}$  and parameter  $L$  from  $\{10, 16, \dots, 40\}$ . In Fig. 3(b), performance is stable for  $L$  within the  $[16, 22]$  range, achieving an ACC of approximately 55.47%. Notably,  $M$  was consistently set to 1000 for all test datasets. To ensure more consistent anchor selection in random sampling, the dataset is sorted in ascending order.

## 4.2. Clustering performance analysis

Tab. 3 reports the clustering performance of various methods on six large-scale multi-view datasets, where the best and second-best are highlighted in **bold** and underlined, respectively. From the table, it is evident that sMERA-MVC and S<sup>2</sup>MVTC significantly outperform others across various metrics such as ACC, NMI, Purity, F-score, PRE, REC, and ARI. sMERA-MVC, leveraging advanced ten-

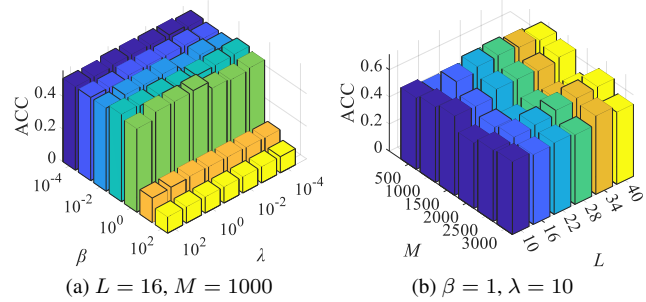


Figure 3. The change of clustering performance as parameters  $\lambda$ ,  $\beta$ , and  $L$ ,  $M$  on Caltech102.

sor networks, excels in exploring both inter-view and intra-view correlations of anchor graphs among views simultaneously. This allows sMERA-MVC to utilize the most compact structure for identifying global correlations among anchor graphs, which could be a key factor contributing to its superior performance.

In comparison with sMERA-MVC, S<sup>2</sup>MVTC consistently outperforms it in most scenarios. Notably, S<sup>2</sup>MVTC demonstrates a significant improvement in clustering performance on the CCV dataset. For instance, the clustering performance of S<sup>2</sup>MVTC has shown remarkable enhancements of 9.25%, 11.17%, and 13.71% in terms of ACC, NMI, and ARI, respectively. In the case of the Caltech102, S<sup>2</sup>MVTC exhibits a performance advantage, achieving a 10.24% higher ACC compared to sMERA-MVC. For the NUS-WIDE-OBJ and AwA datasets, the performances of both methods are similar. Regarding the YoutubeFace\_sel dataset, which is larger than other large-scale datasets, sFSR-IMVC demonstrates the best performance compared to sMERA-MVC.

Significantly, in terms of CPU time, S<sup>2</sup>MVTC outperforms sMERA-MVC across all large datasets, especially with larger sizes. For instance, it achieves an approximation speedup of 39 times on AwA and 20 times on Cifar-10. Furthermore, BMVC, relying on binary feature representation for clustering, exhibits a CPU time performance at a comparable scale to S<sup>2</sup>MVTC on large datasets. However, the clustering performance of S<sup>2</sup>MVTC surpasses BMVC, with ACC improvements of 32.16% on CCV, 25.47% on Caltech102, 48.22% on NUS-WIDE-OBJ, 52.04% on Cifar-10, and 29.18% on YoutubeFace\_sel, respectively.

In summary, based on the analysis of these metrics, it can be concluded that the S<sup>2</sup>MVTC algorithm excels not only in accuracy for multi-view clustering tasks but also significantly outperforms traditional algorithms in terms of computational efficiency, making it suitable for fast large-scale multi-view clustering tasks.

## 4.3. Model discussions

**Model Analysis.** Fig. 4 illustrates the embedding feature learning process of S<sup>2</sup>MVTC on the CCV dataset.

Methods	ACC	NMI	Purity	F-score	PRE	REC	ARI	CPU Time (s)	Speedup
<b>CCV (<math>\beta=0.1, \lambda=10^{-5}, L=18</math>)</b>									
<i>k</i> -means	0.1339	0.0890	0.1680	0.0930	0.0717	0.1321	0.0201	<b>1.12</b>	1x
BMVC (2018)	0.2263	0.2051	0.2612	0.1390	0.1400	0.1380	0.0870	1.95	0.57x
SFMC (2020)	0.1503	0.0904	0.1562	0.1133	0.0637	0.5105	0.0127	17.73	0.06x
OPMC (2021)	0.1955	0.1738	0.2309	0.1176	0.1011	0.1407	0.0546	1.14	0.98x
FPMVS-CAG (2021)	0.2284	0.1670	0.2489	0.1333	0.1212	0.1481	0.0749	11.62	0.10x
FMVACC (2022)	0.1919	0.1505	0.2308	0.1143	0.1201	0.1091	0.0632	31.70	0.03x
FastMICE (2023)	0.2076	0.1623	0.2421	0.1244	0.1264	0.1225	0.0720	17.99	0.06x
FSMSC (2023)	0.2167	0.1799	0.2529	0.1273	0.1348	0.1206	0.0773	4.50	0.25x
sMERA-MVC (2023)	0.4554	0.5002	0.5191	0.3406	0.3508	0.3310	0.3015	3.81	0.29x
S <sup>2</sup> MVTC	<b>0.5479</b>	<b>0.6119</b>	<b>0.5491</b>	<b>0.4784</b>	<b>0.3871</b>	<b>0.6260</b>	<b>0.4386</b>	1.61	0.70x
<b>Caltech102 (<math>\beta=1, \lambda=10, L=16</math>)</b>									
<i>k</i> -means	0.1926	0.4083	0.3822	0.1697	0.2390	0.2390	0.1528	40.38	1.00x
BMVC (2018)	0.3000	0.5096	0.4850	0.2383	0.3496	0.1807	0.2234	7.59	5.32x
SFMC (2020)	0.2440	0.3216	0.2967	0.0547	0.0288	0.5479	0.0012	59.55	0.68x
OPMC (2021)	0.2474	0.4848	0.4509	0.2255	0.3456	0.1673	0.2110	31.67	1.28x
FPMVS-CAG (2021)	0.3118	0.4167	0.3786	0.2530	0.1742	0.4652	0.2211	162.77	0.25x
FMVACC (2022)	0.2440	0.3216	0.2967	0.0547	0.0288	0.5479	0.0012	57.57	0.70x
FastMICE (2023)	0.2408	0.4897	0.4738	0.2042	0.3606	0.1424	0.1913	280.79	0.14x
FSMSC (2023)	0.2757	0.5118	0.4974	0.2196	0.3951	0.1521	0.2072	16.75	2.41x
sMERA-MVC (2023)	0.4523	0.8053	<b>0.7128</b>	0.3585	0.5858	0.2582	0.3472	58.27	0.69x
S <sup>2</sup> MVTC	<b>0.5547</b>	<b>0.8316</b>	0.6667	<b>0.6577</b>	<b>0.6764</b>	<b>0.6400</b>	<b>0.6481</b>	<b>3.56</b>	11.34x
<b>NUS-WIDE-OBJ (<math>\beta=1, \lambda=10^{-3}, L=16</math>)</b>									
<i>k</i> -means	0.1227	0.1050	0.2387	0.0849	0.1070	0.0704	0.0390	60.04	1.00x
BMVC (2018)	0.1573	0.1351	0.2476	0.0972	0.1138	0.0849	0.0483	28.19	2.13x
SFMC (2020)	0.1330	0.0312	0.1356	0.1132	0.0604	0.9066	0.0005	87.09	0.69x
OPMC (2021)	0.1438	0.1523	0.2670	0.0973	0.1236	0.0802	0.0524	22.56	2.66x
FPMVS-CAG (2021)	0.2044	0.1338	0.2348	0.1389	0.1124	0.1817	0.0697	75.76	0.79x
FMVACC (2022)	0.1226	0.1113	0.2230	0.0765	0.1048	0.0602	0.0341	84.44	0.71x
FastMICE (2023)	0.1574	0.1540	0.2611	0.1033	0.1380	0.0825	0.0610	44.41	1.35x
FSMSC (2023)	0.1903	0.1326	0.2263	0.1433	0.1164	0.1866	0.0748	30.88	1.94x
sMERA-MVC (2023)	0.6135	<b>0.8212</b>	<b>0.8244</b>	0.5996	<b>0.7230</b>	0.5122	0.5786	46.15	1.30x
S <sup>2</sup> MVTC	<b>0.6395</b>	0.7440	0.7329	<b>0.6189</b>	0.6280	<b>0.6101</b>	<b>0.5949</b>	<b>8.35</b>	7.19x
<b>AwA (<math>\beta=0.1, \lambda=0.03, L=9</math>)</b>									
<i>k</i> -means	0.0832	0.0951	0.0984	0.0459	0.0366	0.0615	0.0171	802.95	1.00x
BMVC (2018)	0.1049	0.1253	0.1120	0.0533	0.0510	0.0558	0.0296	32.71	24.55x
SFMC (2020)	0.0465	0.0288	0.0474	0.0464	0.0238	0.9587	0.0009	129.57	6.20x
OPMC (2021)	0.0928	0.1193	0.1111	0.0456	0.0449	0.0463	0.0224	182.61	4.40x
FPMVS-CAG (2021)	0.0949	0.1012	0.0997	0.0603	0.0394	0.1282	0.0255	50.81	15.80x
FMVACC (2022)	0.0769	0.0906	0.0988	0.0381	0.0403	0.0361	0.0164	640.66	1.25x
FastMICE (2023)	0.0905	0.1119	0.1114	0.0458	0.0482	0.0435	0.0241	239.61	3.35x
FSMSC (2023)	0.1054	0.1197	0.1259	0.0526	0.0563	0.0493	0.0314	42.51	18.89x
sMERA-MVC (2023)	0.6201	0.7820	<b>0.6888</b>	<b>0.5677</b>	<b>0.5479</b>	0.5889	<b>0.5570</b>	390.59	2.06x
S <sup>2</sup> MVTC	<b>0.6288</b>	<b>0.8124</b>	0.6334	0.5872	0.4735	<b>0.7726</b>	0.5748	<b>10.35</b>	77.58x
<b>Cifar-10 (<math>\beta=10^{-4}, \lambda=10^{-4}, L=16</math>)</b>									
<i>k</i> -means	0.8935	0.7849	0.8935	0.8013	0.7976	0.8050	0.7791	111.04	1.00x
BMVC (2018)	0.9944	0.9846	0.9944	0.9889	0.9889	0.9876	0.9876	12.09	9.19x
SFMC (2020)	0.9873	0.9671	0.9873	0.9750	0.9750	0.9750	0.9722	119.74	0.93x
OPMC (2021)	0.9764	0.9420	0.9764	0.9541	0.9540	0.9542	0.9490	21.33	5.21x
FPMVS-CAG (2021)	0.8969	0.9423	0.8972	0.8953	0.8284	0.9796	0.8822	35.30	3.15x
FMVACC (2022)	0.9646	0.9627	0.9718	0.9588	0.9489	0.9701	0.9540	134.57	0.83x
FastMICE (2023)	0.9920	0.9778	0.9920	0.9842	0.9842	0.9824	0.9824	94.05	1.18x
FSMSC (2023)	0.9954	0.9701	0.9663	0.9564	0.9406	0.9744	0.9512	56.46	1.97x
sMERA-MVC (2023)	<b>1.0000</b>	214.23	0.52x						
S <sup>2</sup> MVTC	0.9994	0.9983	0.9994	0.9989	0.9989	0.9989	0.9988	<b>11.13</b>	9.98x
<b>YoutubeFace_sel (<math>\beta=0.1, \lambda=0.005, L=19</math>)</b>									
<i>k</i> -means	0.1171	0.1025	0.2723	0.0757	0.1068	0.0586	0.0131	1167.73	1.00x
BMVC (2018)	0.2815	0.2818	0.3691	0.1169	0.1911	0.0842	0.0658	<b>36.12</b>	32.33x
SFMC (2020)	0.2843	0.0567	0.2870	0.1665	0.0912	0.9514	0.0039	465.44	2.51x
OPMC (2021)	0.2574	0.2470	0.3467	0.1139	0.1777	0.0838	0.0600	184.88	6.32x
FMVACC (2022)	0.2418	0.2192	0.3329	0.0868	0.1598	0.0596	0.0402	524.17	2.23x
FPMVS-CAG (2021)	0.2510	0.2440	0.3405	0.1305	0.1538	0.1134	0.0591	483.83	2.41x
FastMICE (2023)	0.3029	0.2708	0.3859	0.1189	0.2119	0.0826	0.0723	120.32	9.71x
FSMSC (2023)	0.2398	0.0332	0.2689	0.1583	0.0895	<b>0.6820</b>	0.0002	174.06	6.71x
sMERA-MVC (2023)	0.5381	0.6780	0.7223	0.4279	0.6228	0.3260	0.3906	321.29	3.63x
S <sup>2</sup> MVTC	<b>0.5732</b>	<b>0.8066</b>	<b>0.7943</b>	<b>0.4308</b>	<b>0.7012</b>	0.3109	<b>0.3977</b>	40.09	29.13x

Table 3. The comparison clustering performance on CCV, Caltech102, NUS-WIDE-OBJ, AwA, Cifar-10 and YoutubeFace\_sel datasets.

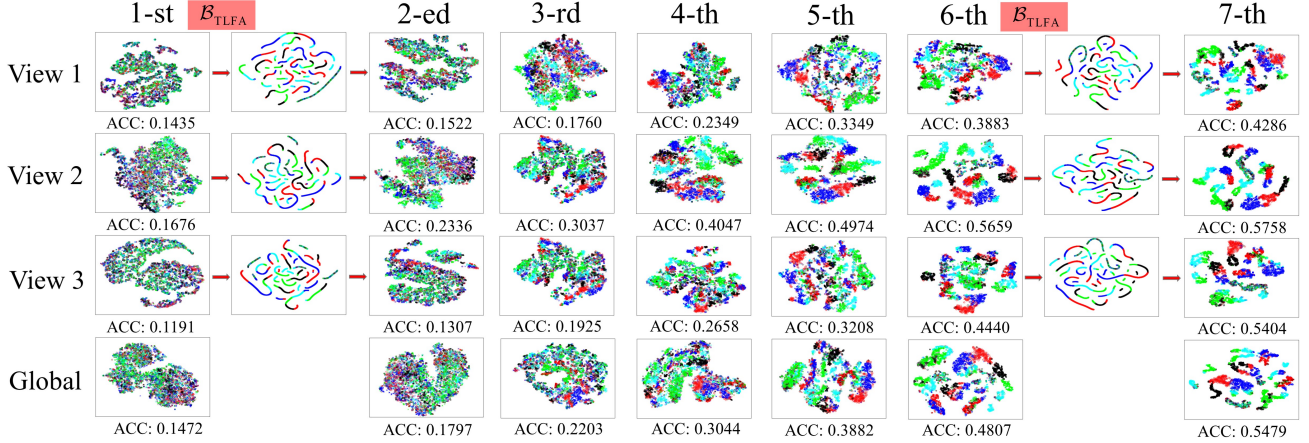


Figure 4. The embedding feature learning process on the CCV dataset. From left to right, the nine columns represent the embedding features after the 1-st iteration, the 1-st TLFA operator, the 2-ed to 6-th iteration, the 6-th TLFA operator, and the 7-th iteration, respectively. Each feature is visualized using t-SNE [33]: View 1 for SIFT features, View 2 for STIP features, View 3 for MFCC features, and ‘Global’ for the fusion of these features.

Compared the 1-st and 3-rd columns, it is evident that after the TLFA operation, the dispersion of sample points increases. This is because that TLFA aims at identifying the compact subspace representation of embedding features across views, known as a smooth representation. During the iterative process, the complementary information captured in this compact subspace further propagates across views. Simultaneously, the exploration of complementary information facilitates the discovery of improved and more smooth subspace representations, ultimately resulting in enhanced clustering performance. For instance, after the 6-th TLFA operation, the clustering performance reaches 54.79%.

**Ablation Study.** The  $S^2$ MVTC model consists primarily of three components: 1. Exploration of ISC; 2. Exploration of IGS; 3. Adoption of a nonlinear anchor graph. To further investigate why  $S^2$ MVTC performs well, we systematically removed each component while keeping the other two fixed, naming these methods as w/o ISC, w/o IGS, and linear anchor graphs. The results are presented in Tab. 4. From the table, it can be observed that removing the exploration of ISC leads to a slight decline in clustering performance, while the removal of the exploration of IGS results in a significant drop in clustering performance. This indicates that the comprehensive exploration of graph similarity among intra-view features effectively, thereby improving clustering performance. Furthermore, when the anchor graph is transformed into a linear mapping between anchors and samples, clustering performance decreases with an increase in the number of samples, especially in Cifar-10 and YoutubeFace\_sel. This is because, with a fixed number of anchors, a nonlinear anchor graph is better at capturing relationships between samples when the sample size is ex-

ceptionally large.

Dataset	w/o ISC		w/o IGS		linear anchor graphs		$S^2$ MVTC	
	ACC	ACC	ACC	ACC	ACC	ACC	ACC	ACC
CCV	54.42	15.49	47.31	54.79				
Caltech102	51.31	17.27	44.71	55.47				
NUS-WIDE-OBJ	63.06	17.17	63.21	63.95				
AwA	51.61	8.08	58.97	62.53				
Cifar-10	99.94	65.92	88.25	99.94				
YoutubeFace_sel	53.97	11.38	40.20	57.33				

Table 4. Ablation Studies on six large-scale datasets.

## 5. Conclusion

In this paper, we present a simple yet efficient scalable multi-view tensor clustering, where the intra-view and inter-view correlations are directly learned from the embedding features. During the iterative process, the introduced TLFA operator optimizes the embedding features to a compact subspace. This optimization aids in exploring complementary information and its propagation across multiple independent views, ensuring maximum consistency between different views. Additionally, we incorporate inter-view semantic consistency and a nonlinear anchor graph to enhance clustering performance. Numerical experiments on six large-scale multi-view datasets demonstrate that our method outperforms all state-of-the-art methods, showcasing a notable improvement with increasing data size.

## References

- [1] Tadas Baltrušaitis, Chaitanya Ahuja, and Louis-Philippe Morency. Multimodal machine learning: A survey and taxonomy. *TPAMI*, 41(2):423–443, 2018. 1
- [2] Karen Braman. Third-order tensors as linear operators on a space of matrices. *Linear Algebra and its Applications*, 433 (7):1241–1253, 2010. 2

[3] Erica L Busch, Jessie Huang, Andrew Benz, Tom Wallenstein, Guillaume Lajoie, Guy Wolf, Smita Krishnaswamy, and Nicholas B Turk-Browne. Multi-view manifold learning of human brain-state trajectories. *Nature Computational Science*, 3(3):240–253, 2023. 1

[4] Man-Sheng Chen, Chang-Dong Wang, and Jian-Huang Lai. Low-rank tensor based proximity learning for multi-view clustering. *TKDE*, 2022. 1

[5] Zhe Chen, Xiao-Jun Wu, Tianyang Xu, and Josef Kittler. Fast self-guided multi-view subspace clustering. *TIP*, pages 1–1, 2023. 3

[6] Zhe Chen, Xiao-Jun Wu, Tianyang Xu, and Josef Kittler. Fast self-guided multi-view subspace clustering. *TIP*, 2023. 6

[7] Tat-Seng Chua, Jinhui Tang, Richang Hong, Haojie Li, Zhiping Luo, and Yan-Tao Zheng. Nus-wide: A real-world web image database from national university of singapore. In *Proc. of ACM Conf. on Image and Video Retrieval (CIVR'09)*, Santorini, Greece., July 8-10, 2009. 5

[8] Han Hu et al. Smooth representation clustering. In *CVPR*, pages 3834–3841, 2014. 2

[9] Dong Huang, Chang-Dong Wang, and Jian-Huang Lai. Fast multi-view clustering via ensembles: Towards scalability, superiority, and simplicity. *TKDE*, 35(11):11388–11402, 2023. 3

[10] Dong Huang, Chang-Dong Wang, and Jian-Huang Lai. Fast multi-view clustering via ensembles: Towards scalability, superiority, and simplicity. *TKDE*, 2023. 5

[11] René J Huster, Stefan Debener, Tom Eichele, and Christoph S Herrmann. Methods for simultaneous eeg-fmri: an introductory review. *Journal of Neuroscience*, 32(18): 6053–6060, 2012. 1

[12] Jintian Ji and Songhe Feng. Anchor structure regularization induced multi-view subspace clustering via enhanced tensor rank minimization. In *ICCV*, pages 19343–19352, 2023. 1, 3

[13] Yu-Gang Jiang, Guangnan Ye, Shih-Fu Chang, Daniel Ellis, and Alexander C. Loui. Consumer video understanding: A benchmark database and an evaluation of human and machine performance. In *ICMR*, 2011. 5

[14] Zhao Kang, Wangtao Zhou, Zhitong Zhao, Junming Shao, Meng Han, and Zenglin Xu. Large-scale multi-view subspace clustering in linear time. In *AAAI*, pages 4412–4419, 2020. 3

[15] M. Kilmer, K. Braman, N. Hao, and R. Hoover. Third-order tensors as operators on matrices: A theoretical and computational framework with applications in imaging. *SIAM J. Matrix Anal. Appl.*, 34(1):148–172, 2013. 2

[16] Misha E Kilmer and Carla D Martin. Factorization strategies for third-order tensors. *Linear Algebra and its Applications*, 435(3):641–658, 2011. 2

[17] Alex Krizhevsky. Learning multiple layers of features from tiny images. 2012. 5

[18] Christoph H. Lampert, Hannes Nickisch, and Stefan Harmeling. Attribute-based classification for zero-shot visual object categorization. *TPAMI*, 36(3):453–465, 2014. 5

[19] Fei-Fei Li, Marco Andreetto, Marc’Aurelio Ranzato, and Pietro Perona. Caltech 101, 2022. 5

[20] X. Li, H. Zhang, R. Wang, and F. Nie. Multiview clustering: A scalable and parameter-free bipartite graph fusion method. *TPAMI*, 44(1):330–344, 2020. 1, 5

[21] Xuelong Li, Han Zhang, Rong Wang, and Feiping Nie. Multiview clustering: A scalable and parameter-free bipartite graph fusion method. *TPAMI*, 44(1):330–344, 2022. 3

[22] Xingfeng Li, Zhenwen Ren, Quansen Sun, and Zhi Xu. Auto-weighted tensor schatten p-norm for robust multi-view graph clustering. *PR*, 134:109083, 2023. 1

[23] Jiyuan Liu, Xinwang Liu, Yuexiang Yang, Li Liu, Siqi Wang, Weixuan Liang, and Jiangyong Shi. One-pass multi-view clustering for large-scale data. In *ICCV*, pages 12344–12353, 2021. 5

[24] Zhen Long, Ce Zhu, Jie Chen, Zihan Li, Yazhou Ren, and Yipeng Liu. Multi-view mera subspace clustering. *TMM*, pages 1–11, 2023. 1, 3, 6

[25] Canyi Lu, Jia Shi Feng, Yudong Chen, Wei Liu, Zhouchen Lin, and Shuicheng Yan. Tensor robust principal component analysis with a new tensor nuclear norm. *TPAMI*, 42(4):925–938, 2020. 2

[26] Christoph Mülert and Louis Lemieux. *EEG-fMRI: physiological basis, technique, and applications*. Springer Nature, 2023. 1

[27] Benjamin Recht. A simpler approach to matrix completion. *JMLR*, 12(12), 2011. 2

[28] Walter Rudin et al. *Principles of mathematical analysis*. McGraw-hill New York, 1976. 5

[29] Angela Serra, Paola Galdi, and Roberto Tagliaferri. Multi-view learning in biomedical applications. In *Artificial intelligence in the age of neural networks and brain computing*, pages 307–324. Elsevier, 2024. 1

[30] X. Shu, X. Zhang, Q. Gao, M. Yang, R. Wang, and X. Gao. Self-weighted anchor graph learning for multi-view clustering. *TMM*, 2022. 1

[31] Xiaomeng Si, Qiyue Yin, Xiaojie Zhao, and Li Yao. Consistent and diverse multi-view subspace clustering with structure constraint. *PR*, 121:108196, 2022. 1

[32] Shiliang Sun. A survey of multi-view machine learning. *Neural computing and applications*, 23:2031–2038, 2013. 1

[33] Laurens Van der Maaten and Geoffrey Hinton. Visualizing data using t-sne. *JMLR*, 9(11), 2008. 8

[34] U. Von Luxburg. A tutorial on spectral clustering. *Statistics and computing*, 17(4):395–416, 2007. 1

[35] Huibing Wang, Mingze Yao, Guangqi Jiang, Zetian Mi, and Xianping Fu. Graph-collaborated auto-encoder hashing for multiview binary clustering. *TNNLS*, pages 1–13, 2023. 1, 4

[36] Nan Wang, Dongren Yao, Lizhuang Ma, and Mingxia Liu. Multi-site clustering and nested feature extraction for identifying autism spectrum disorder with resting-state fmri. *Medical image analysis*, 75:102279, 2022. 1

[37] S. Wang, X. Liu, X. Zhu, P. Zhang, Y. Zhang, F. Gao, and E. Zhu. Fast parameter-free multi-view subspace clustering with consensus anchor guidance. *TKDE*, 31:556–568, 2021. 1, 6

[38] Siwei Wang, Xinwang Liu, Suyuan Liu, Jiaqi Jin, Wenxuan Tu, Xinzhong Zhu, and En Zhu. Align then fusion: Generalized large-scale multi-view clustering with anchor matching correspondences. *NeurIPS*, 35:5882–5895, 2022. 5

- [39] Siwei Wang, Xinwang Liu, Xinzhang Zhu, Pei Zhang, Yi Zhang, Feng Gao, and En Zhu. Fast parameter-free multi-view subspace clustering with consensus anchor guidance. *TIP*, 31:556–568, 2022. [1](#), [3](#)
- [40] J. Wen, Z. Zhang, Z. Zhang, L. Zhu, L. Fei, B. Zhang, and Y. Xu. Unified tensor framework for incomplete multi-view clustering and missing-view inferring. In *Proc. AAAI Conf. Artif. Intell.*, pages 10273–10281, 2021. [4](#)
- [41] Lior Wolf, Tal Hassner, and Itay Maoz. Face recognition in unconstrained videos with matched background similarity. In *CVPR*, 2011. [5](#)
- [42] W. Xia, Q. Gao, Q. Wang, X. Gao, C. Ding, and D. Tao. Tensorized bipartite graph learning for multi-view clustering. *TPAMI*, 2022. [1](#), [3](#)
- [43] M. Yang, P. Li, Y. and Hu, J. Bai, J. Lv, and X. Peng. Robust multi-view clustering with incomplete information. *TPAMI*, 45(1):1055–1069, 2022. [1](#)
- [44] Yachao Zhang, Yuan Xie, Cuihua Li, Zongze Wu, and Yanyun Qu. Learning all-in collaborative multiview binary representation for clustering. *TNNLS*, pages 1–14, 2022. [1](#), [4](#)
- [45] Zheng Zhang, Li Liu, Fumin Shen, Heng Tao Shen, and Ling Shao. Binary multi-view clustering. *TPAMI*, 41(7):1774–1782, 2018. [1](#), [4](#), [5](#)